

Phase structure of $N_f = 3$ QCD at finite temperature and density by Wilson-Clover fermions

Shinji Takeda^{*a,b,†}, Xiao-Yong Jin^c, Yoshinobu Kuramashi^{b,d,e}, Yoshifumi Nakamura^b, and Akira Ukawa^b

^a *Institute of Physics, Kanazawa University, Kanazawa 920-1192, Japan*

^b *RIKEN Advanced Institute for Computational Science, Kobe, Hyogo 650-0047, Japan*

^c *Argonne Leadership Computing Facility, Argonne National Laboratory, Argonne, IL 60439, USA*

^d *Graduate School of Pure and Applied Sciences, University of Tsukuba, Tsukuba, Ibaraki 305-8571, Japan*

^e *Center for Computational Sciences, University of Tsukuba, Tsukuba, Ibaraki 305-8577, Japan*

We investigate the phase structure of 3-flavor QCD in the presence of finite quark chemical potential by using Wilson-Clover fermions. To deal with the complex action with finite density, we adopt the phase reweighting method. In order to survey a wide parameter region, we employ the multi-parameter reweighting method as well as the multi-ensemble reweighting method. Especially, we focus on locating the critical end point that characterizes the phase structure. It is estimated by the kurtosis intersection method for the quark condensate. For Wilson-type fermions, the correspondence between bare parameters and physical parameters is indirect, thus we present a strategy to transfer the bare parameter phase structure to the physical one. We conclude that the curvature with respect to the chemical potential is positive. This implies that, if one starts from a quark mass in the region of crossover at zero chemical potential, one would encounter a first-order phase transition when one raises the chemical potential.

*The 33rd International Symposium on Lattice Field Theory
14 -18 July 2015
Kobe International Conference Center, Kobe, Japan*

^{*}Speaker.

[†]E-mail: takeda@hep.s.kanazawa-u.ac.jp

1. Introduction

The location of the critical end point in the QCD phase diagram at finite density is an important unsolved issue. In this article, we address the issue of how the critical end line extends when switching on the quark chemical potential. An interesting result was reported in [1, 2] which explored the imaginary chemical potential approach with the naive staggered fermion action. There it was reported that the critical surface has a negative curvature in the μ direction. This means that a first-order phase transition at zero chemical potential disappears when the chemical potential is increased, rather contrary to one's naive guess. Our purpose in this report is to study this question by simulations with real chemical potential using the Wilson-clover fermion action. The detail of this article can be seen in [3].

2. Strategy

In this section, we explain our strategy to survey the phase space for $N_f = 3$ QCD, especially how to identify the critical end point for the Wilson-type fermions and how to obtain the curvature of the critical end line on the μ - m_π plane. Note that in this section we do not use lattice units when expressing dimensionful physical quantities.

First we consider the zero density case. Since the quark masses are all degenerate, we have only two bare parameters β and κ ($a\mu = 0$ plane in the left panel in Fig. 1). For a given temporal lattice size, say $N_t = 4$, by using the peak position of susceptibility of quark condensate, one can draw the line of finite temperature transition. The transition changes from being of first order to cross over at a second order critical end point. We compute the kurtosis of quark condensate along the transition line for a set of spatial volumes. The intersection point is identified as the critical end point [4]. In this way, we can determine the critical end point in the bare parameter space (β_E, κ_E) and this procedure can be repeated for other values of N_t .

In order to translate the critical end point in the bare parameter space to that in the physical parameter space, we measure dimensionless ratios of pseudo-scalar meson mass and some reference quantity with mass-dimension one m_{PS}/Λ for the bare parameters (β_E, κ_E) by a zero temperature simulation. To avoid the multiplicative renormalization, we use m_{PS} in the numerator of the ratio and not quark masses. In this way we pin down the critical end point in the physical parameter space. By repeating the same calculation for increasingly larger values of N_t , we can take the continuum limit of the critical end point (this strategy is in fact used in our zero density study [6]),

$$\frac{m_{PS,E}^{\text{cont}}(\mu = 0)}{\Lambda_E^{\text{cont}}(\mu = 0)} = \lim_{N_t \rightarrow \infty} \frac{m_{PS,E}(\mu = 0)}{\Lambda_E(\mu = 0)}. \quad (2.1)$$

When switching on the chemical potential, the basic procedure is the same; one just has to repeat the same analysis on a different plane with $\mu \neq 0$ (see the left panel in Fig. 1). For a fixed lattice temporal size, $N_t = 6$, in order to draw the critical end line, we consider a pair of dimensionless ratios

$$\frac{m_{PS,E}(\mu)}{m_{PS,E}(0)} \quad \text{and} \quad \frac{\mu}{T_E(0)}, \quad (2.2)$$

where for each ratio we have chosen proper reference quantities at zero density. By plotting these two quantities one can obtain a critical line as shown in the right panel of Fig. 1. Especially, we are

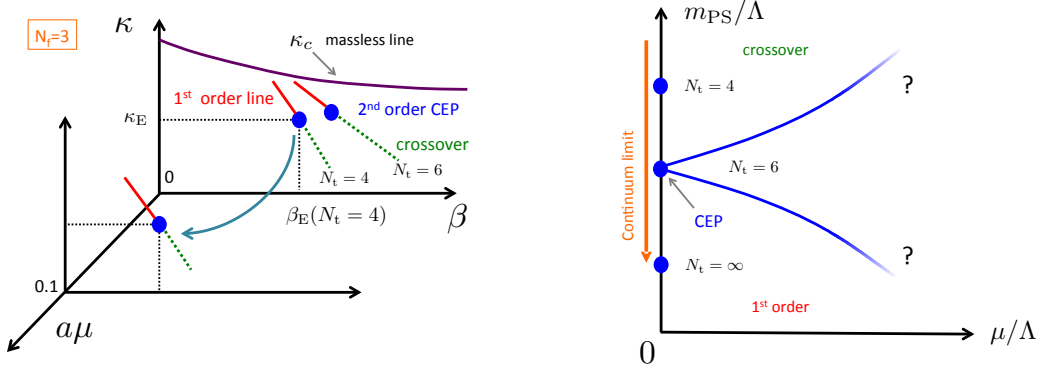


Figure 1: Strategy: The left panel is the phase diagram for bare parameters spanned by β , κ and $a\mu$ for $N_f = 3$. The right panel is the same phase diagram but depicted for physical parameters spanned by m_{PS}/Λ and μ/Λ where Λ is some reference physical quantity at zero density. The blue line is the critical line. We study the signature of the curvature of critical line with fixed $N_t = 6$.

interested the curvature α_1 of the fitting form

$$\left(\frac{m_{PS,E}(\mu)}{m_{PS,E}(0)}\right)^2 = 1 + \alpha_1 \left(\frac{\mu}{\pi T_E(0)}\right)^2 + \alpha_2 \left(\frac{\mu}{\pi T_E(0)}\right)^4 + \dots \quad (2.3)$$

3. Simulation details

We employ the Wilson-clover fermion action with non-perturbatively tuned c_{sw} [7] in the presence of chemical potential. The Iwasaki gauge action [8] is used for the gluon sector. The number of flavor is three, $N_f = 3$, and the masses and chemical potentials for quarks are all degenerate. The temporal lattice size and the simulated quark chemical potential are fixed to $N_t = 6$ and $a\mu = 0.1$, respectively. In our study, the phase reweighting method is used to deal with the complex phase. To survey a wide range of μ and κ , we adopt the multi-parameter reweighting method. To perform finite size scaling analysis, the spatial volume is changed over the linear sizes $N_s = 8, 10$ and 12 . In order to search for the transition point, we select four β points ($\beta = 1.70, 1.73, 1.75$ and 1.77) and for each β , we vary κ to locate the transition point.

Configurations are generated by RHMC with the phase quenched quark determinant. For each lattice parameter set $(\beta, \kappa, N_t, N_s)$ we generate $O(100,000)$ trajectories, with the configurations stored at every 10th trajectory. The phase factor is computed exactly using the analytical reduction technique [9, 10, 11] for all stored configurations. The dense matrix obtained by the reduction is numerically computed on GPGPU with LAPACK routines. We measure the trace of quark propagator and its higher power up to fourth order which are used not only for the computation of higher moments of quark condensate but also for the parameter reweighting. In the computation of traces, we adopt the noise method with 20 Gaussian noises that is checked to be sufficient to control the noise error.

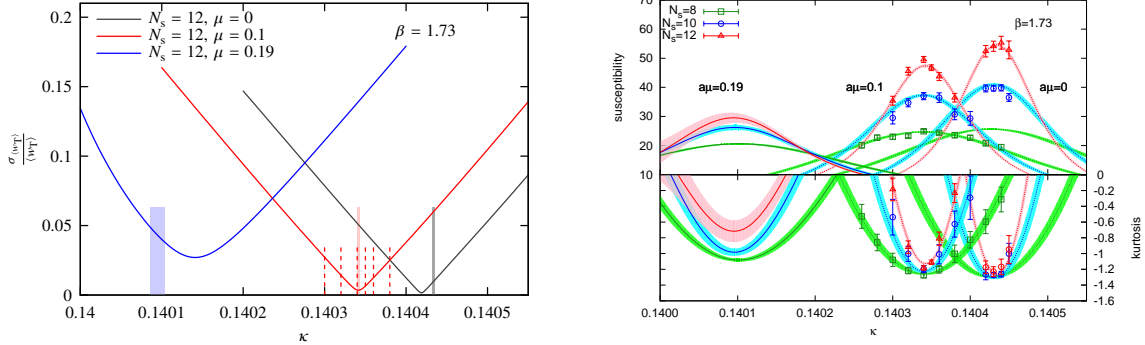


Figure 2: The left panel is the relative error of the reweighting factor of multi-ensemble reweighting as a function of κ for 1.73. Here only three selected values of the chemical potential are shown for each β . The spatial lattice is fixed $N_s = 12$. The right panel is the susceptibility and kurtosis of quark condensate as a function of κ for 1.73. In $\beta = 1.73$ with $N_s = 10, 12$, we also plot the raw data at $a\mu = 0$ given in the zero density study [6].

For each fixed parameter set $(\beta, a\mu, N_t, N_s)$, we make runs at several values of κ . In order to integrate those runs we adopt the multi-ensemble reweighting technique [12] and search for the transition point in κ for the fixed parameter set. We employ some approximation, checking its validity numerically, to efficiently evaluate the quark determinant in the reweighting factor as well as observables at many reweighting points.

4. Simulation results

The relative error of the reweighting factor of the multi-ensemble reweighting is plotted in Fig. 2 (left panel). The relative error takes small values even at a large chemical potential $a\mu \approx 0.2$, and the reweighting factor is significantly away from zero beyond several sigmas. Thus we conclude that the overlap problem is not so severe in our parameter region.

The right panel of Fig. 2 shows curves of the susceptibility and kurtosis for quark condensate obtained by the multi-ensemble reweighting. For $a\mu = 0.1$, the averages at each point of data generation are shown in order to illustrate how multi-ensemble curves interpolate those raw data. At $\beta = 1.73$, the curves reweighted to $a\mu = 0$ can be compared with data generated at zero density [6]. The agreement supports the validity of multi-ensemble reweighting and jackknife error estimation away from $a\mu = 0.1$. The applicable range of μ/κ -reweighting depends on β , and judged from the growth of error, the lower β tends to have a larger applicable range. As seen in the figure, the locations of the maximum of susceptibility and minimum of kurtosis are consistent with each other. We take the location of the maximum of susceptibility as the transition point. We observe that the volume dependence of the transition points is rather mild. Hence the thermodynamic limit can be safely taken with a fitting ansatz, $\kappa_t(N_s) = \kappa_t(\infty) + c/N_s^3$. The phase diagram of bare parameters β and κ is given in Fig. 3.

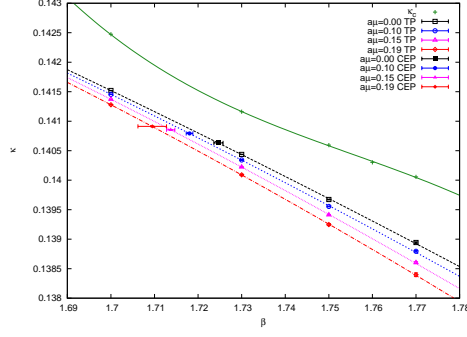


Figure 3: The phase diagram of $N_f = 3$ QCD with finite chemical potential projected on the (β, κ) plane. The transition points are expressed by open symbol while the critical end points are given by filled one. The lower β side of the critical end point is the first order phase transition region. The κ_c line where the pion mass vanishes is also shown.

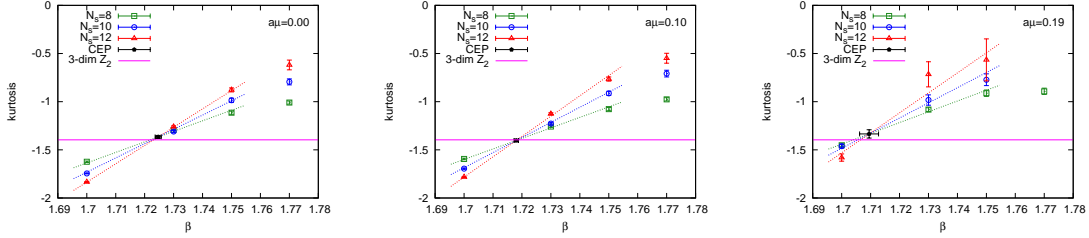


Figure 4: Kurtosis intersection at $a\mu = 0.00 - 0.19$. In the fitting, three lowest values of β are used. The black pentagon represents the critical end point (CEP) in bare parameter space and it moves to lower side for larger chemical potential. The horizontal line shows $K_E = -1.396$ for 3-D Z_2 universality class.

The next step is to determine the critical end point. For that purpose we adopt the kurtosis intersection method [4]. Figure 4 plots the minimum of kurtosis as a function of β for some selected values of $a\mu$. This shows that a strong first order phase transition at lower β becomes weaker for higher β and such a change becomes rapid for larger volumes. We fit the data with the fitting form [1] inspired by finite size scaling, $K_{\min} = K_E + AN_s^{1/\nu}(\beta - \beta_E)$, where K_E , A , ν and β_E are fitting parameters. We observe that the resulting exponent ν and the value of kurtosis at the critical end point K_E are independent of $a\mu$ within errors, and they are consistent with the values of 3-D Z_2 universality class, $\nu = 0.63$ and $K_E = -1.396$ respectively. On the other hand, the universality class of 3-dimensional $O(2)$ and 3-dimensional $O(4)$ are rejected, rather strongly by the value of K_E . We superimpose the obtained critical end points $(\beta_E(a\mu), \kappa_E(a\mu))$ for $0 \leq a\mu \leq 0.19$ in the phase diagram of Fig. 3.

5. Critical line and its curvature

The analysis of the critical line below requires a careful manipulation with scale setting. Thus we distinguish quantities in lattice units from those in physical units by placing tilde on the former, *e.g.*, chemical potential in physical units is denoted as μ and that in lattice units by $\tilde{\mu} = a\mu$.

In the previous section, we have determined the critical end points in the bare parameter space. We now translate the critical end point on the (β, κ) plane to the physical space, to obtain the critical line as one varies μ , and finally to extract its curvature. For that purpose, as explained in Sect. 2, we need to compute the pair of ratios in eq.(2.2) as follows,

$$\frac{m_{\text{PS,E}}(\mu)}{m_{\text{PS,E}}(0)} = \frac{\tilde{m}_{\text{PS,E}}(\tilde{\mu})}{\tilde{m}_{\text{PS,E}}(0)} \cdot \frac{a(0)}{a(\tilde{\mu})}, \quad \frac{\mu}{T_{\text{E}}(0)} = \tilde{\mu} \cdot \frac{a(0)}{a(\tilde{\mu})} \cdot N_t, \quad (5.1)$$

where $\tilde{m}_{\text{PS,E}}(\tilde{\mu})$ is the pseudo-scalar (PS) meson mass in lattice units evaluated at $(\beta, \kappa) = (\beta_{\text{E}}(\tilde{\mu}), \kappa_{\text{E}}(\tilde{\mu}))$. The PS mass is measured by the zero temperature simulation at β_{E} and κ_{E} . On the other hand, the lattice spacing requires some careful thought as follows.

We usually determine the lattice spacing by choosing a line of constant physics (LCP) and specifying the value of a dimensionful physical quantity on that line. For example, one may choose the dimensionless combination $m_{\text{PS}}\sqrt{t_0}$ for specifying the LCP, and the value of m_{PS} in physical units to determine the lattice spacing along the chosen LCP,

$$a(\beta, y) = \frac{\tilde{m}_{\text{PS}}(\beta, \kappa_y(\beta))}{m_{\text{PS}}(y)}, \quad (5.2)$$

where y is the value of the constant physics $y = m_{\text{PS}}\sqrt{t_0}$ and $\kappa_y(\beta)$ is defined such that $y = \tilde{m}_{\text{PS}}(\beta, \kappa_y(\beta))\sqrt{t_0}(\beta, \kappa_y(\beta))$ holds for each β . The notation of the lattice spacing in eq.(5.1) means that $a(\tilde{\mu}) = a(\beta_{\text{E}}(\tilde{\mu}), y)$. Along LCP, where the physical unit mass in the denominator in eq.(5.2) is not known a priori but common, the physical mass cancels out in the ratio of lattice spacings and the ratio may be computed by using the PS mass in lattice units,

$$\frac{a(0)}{a(\tilde{\mu})} = \frac{\tilde{m}_{\text{PS}}(\beta_{\text{E}}(0), \kappa_y(\beta_{\text{E}}(0)))}{\tilde{m}_{\text{PS}}(\beta_{\text{E}}(\tilde{\mu}), \kappa_y(\beta_{\text{E}}(\tilde{\mu})))}. \quad (5.3)$$

In the following, for the computation of the ratio of lattice spacings, we use the Wilson flow scale instead of the PS mass since the former is more precisely calculated

$$\frac{a(0)}{a(\tilde{\mu})} = \frac{1/\sqrt{t_0}(\beta_{\text{E}}(0), \kappa_y(\beta_{\text{E}}(0)))}{1/\sqrt{t_0}(\beta_{\text{E}}(\tilde{\mu}), \kappa_y(\beta_{\text{E}}(\tilde{\mu})))}. \quad (5.4)$$

One can employ a different LCP by specifying a different value of $y' (\neq y)$. The resulting lattice spacing coincides with that from the original (y) definition if, in specifying the value of the dimensionful quantity, one takes into account the variation of that quantity in moving from the original LCP to a new LCP. In general the agreement will not be exact due to scaling violations. Thus differences one may observe in physical results due to the choice of LCP is a scaling violation effect. In the following, we choose two values for the line of constant physics, namely, $y = m_{\text{PS}}\sqrt{t_0} = 0.55$ and 0.65 .

We use the Wilson flow scale and the hadron mass computed in Appendix A of Ref. [6]. By combining the above scale inputs and the information of critical end point at finite chemical potential determined in the previous section, we calculate the two ratios in eq.(5.1). The results are plotted in Fig. 5. We extract the curvature by using the fitting form in eq.(2.3). We find the curvature values as given by

$$\alpha_1 = \begin{cases} 1.924(60) & \text{for } y = 0.55, \\ 2.148(39) & \text{for } y = 0.65. \end{cases} \quad (5.5)$$

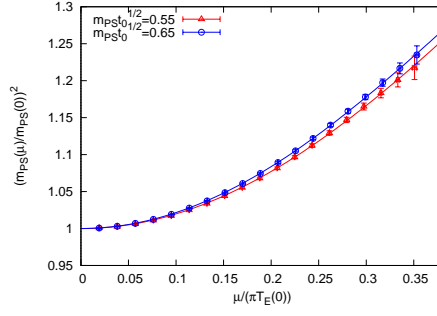


Figure 5: Critical line for constant physics $y = m_{\text{PSt}_0}^{1/2} = 0.55, 0.65$ with scale input: the Wilson flow scale.

We observe that the critical line has a sensitivity on the value of y . This difference is considered as a systematic uncertainty caused by the choice of the scale setting as discussed above. All in all, we find the curvature of the critical line to be positive with a statistical error of about 3% and a systematic error of about 10%.

This research used computational resources of the K computer provided by the RIKEN Advanced Institute for Computational Science through the HPCI System Research project (Project ID:hp120115), and the HA-PACS provided by Interdisciplinary Computational Science Program in Center for Computational Sciences, University of Tsukuba. This work is supported by JSPS KAKENHI Grant Numbers 23740177 and 26800130. This work was supported by FOCUS Establishing Supercomputing Center of Excellence.

References

- [1] P. de Forcrand and O. Philipsen, JHEP **0701**, 077 (2007) [hep-lat/0607017].
- [2] P. de Forcrand, S. Kim and O. Philipsen, PoS LAT **2007**, 178 (2007) [arXiv:0711.0262 [hep-lat]].
- [3] X. Y. Jin, Y. Kuramashi, Y. Nakamura, S. Takeda and A. Ukawa, arXiv:1504.00113 [hep-lat].
- [4] F. Karsch, E. Laermann and C. Schmidt, Phys. Lett. B **520**, 41 (2001) [hep-lat/0107020].
- [5] M. Lüscher, JHEP **1008**, 071 (2010), [arXiv:1006.4518 [hep-lat]].
- [6] X. Y. Jin *et al.*, Phys. Rev. D **91**, no. 1, 014508 (2015) [arXiv:1411.7461 [hep-lat]].
- [7] CP-PACS/JLQCD Collaborations (S. Aoki *et al.*), Phys. Rev. D **73**, 034501 (2006) [hep-lat/0508031].
- [8] Y. Iwasaki, Report No. UTHEP-118 (1983), [arXiv:1111.7054].
- [9] J. Danzer and C. Gattringer, Phys. Rev. D **78**, 114506 (2008) [arXiv:0809.2736 [hep-lat]].
- [10] S. Takeda, Y. Kuramashi and A. Ukawa, Phys. Rev. D **85**, 096008 (2012) [arXiv:1111.6363 [hep-lat]].
- [11] S. Takeda, Y. Kuramashi and Y. Nakamura AICS Technical Report No. 2015-001.
- [12] A. M. Ferrenberg and R. H. Swendsen, Phys. Rev. Lett. **61**, 2635 (1988).